iScience, Volume *26*

Supplemental information

Flat clathrin lattices are linked to metastatic potential in colorectal cancer

Charlotte Cresens, Guillermo Solís-Fernández, Astha Tiwari, Rik Nuyts, Johan Hofkens, Rodrigo Barderas, and Susana Rocha

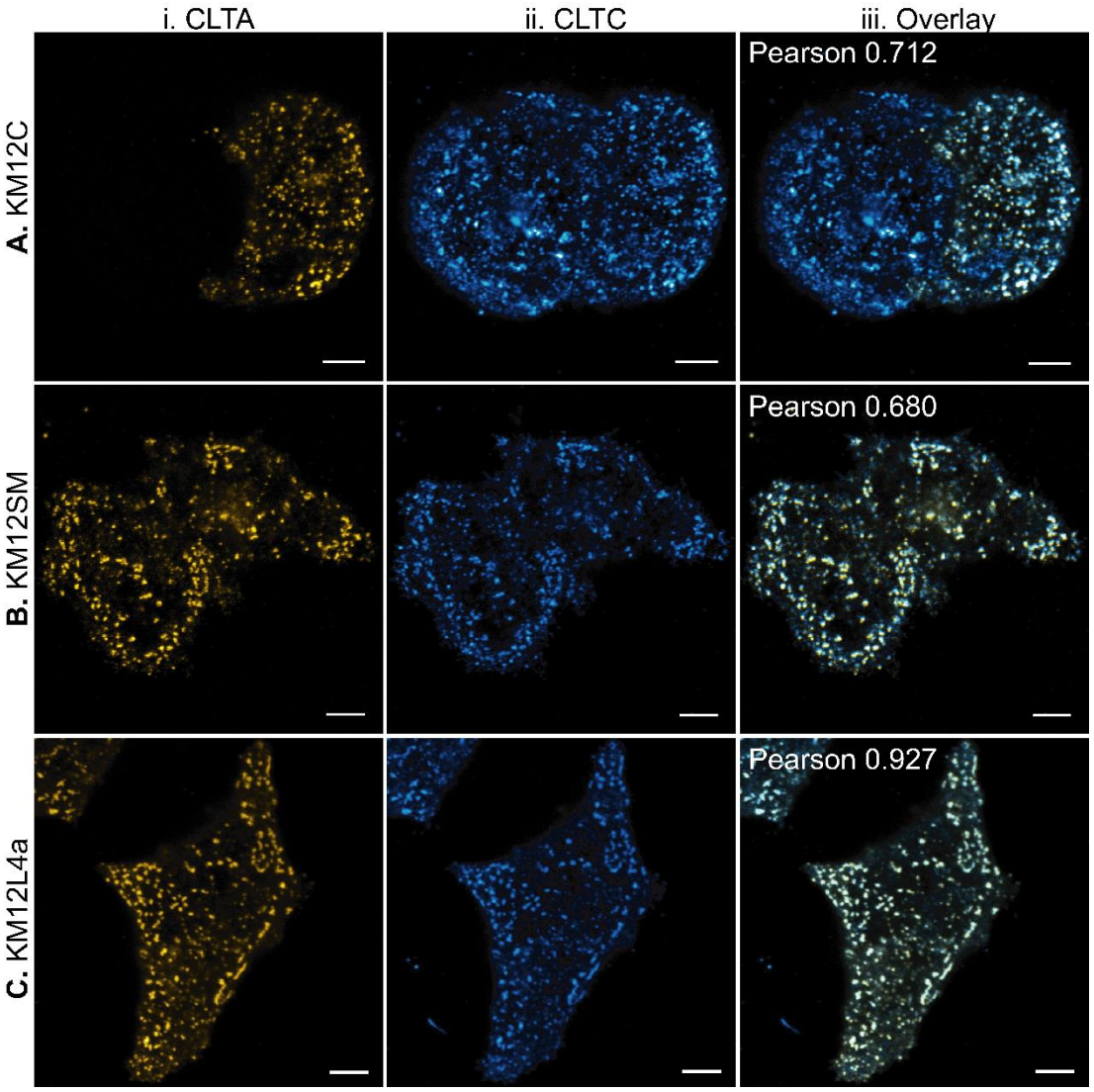

Figure S1: Comparison of clathrin transfection and immunolabeling, related to Figure 1. Representative dual-color images of transiently transfected EYFP-CLTA (i) and immunolabeled Atto647N-CLTC (ii) at the ventral membrane of poorly metastatic KM12C (A), metastatic KM12SM (B) and metastatic KM12L4a (C) cells. Images were taken sequentially for the same field of view. Overlays (iii) show a very comparable clathrin topology between transfection and immunolabeling conditions, as quantified by the Pearson Correlation Coefficient of the transfected cell. Scale bars 5 µm.

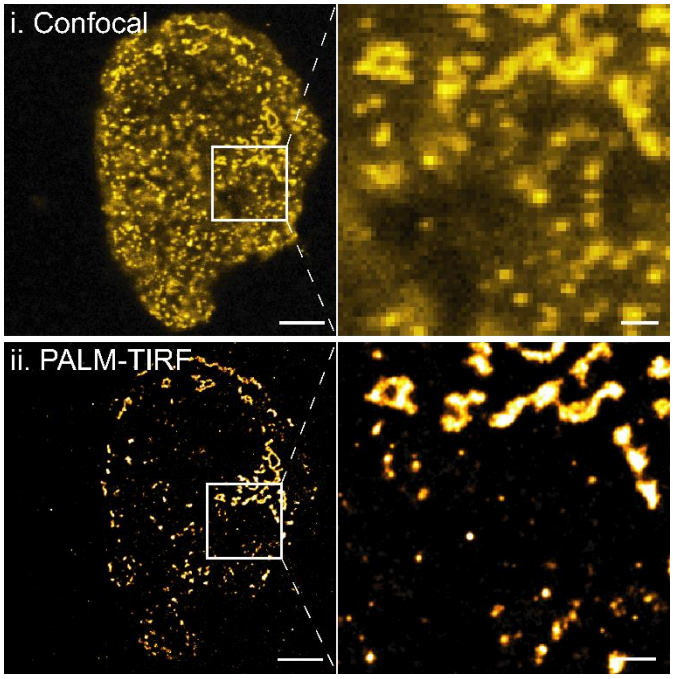

Figure S2: Comparison of confocal and PALM-TIRF microscopy for clathrin imaging at the ventral membrane, related to Figure 3 and Figure 4. The same metastatic KM12L4a cell transfected with mEos3.2-CLTA was imaged using confocal microscopy (i) and PALM-TIRF microscopy (ii). Note that CCSs in the cytoplasm are visible (as out-of-focus structures) in the confocal image, while the PALM-TIRF image contains only CCSs that are truly located at the ventral membrane due to the enhanced axial resolution in TIRF-mode. Scale bars 5 µm, except scale bars of enlargements 1 µm.

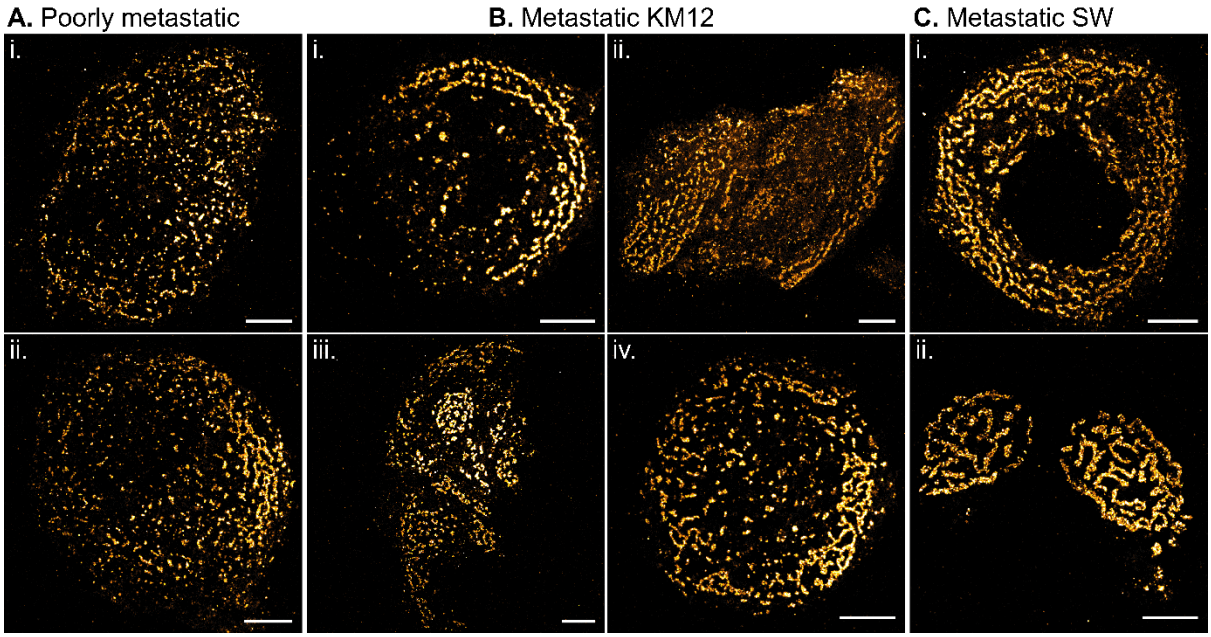

Figure S3: Variability of clathrin topology (mEos3.2-CLTA) at the ventral membrane of the KM12 and SW models, imaged with PALM-TIRF microscopy, related to Figure 4. Images representative of the variability found within poorly metastatic cells (A), within metastatic KM12 cells (B) and within metastatic SW cells (C) are shown. Poorly metastatic cells predominantly display classical CCSs (Ai), however, occasionally certain membrane regions also exhibit alternative FCLs (Aii), but to a far less extent than in the metastatic cells. Especially in the metastatic cells lines there is a larger discrepancy in clathrin distribution since FCLs in the metastatic KM12 cells can be arranged in concentric rings following the cell periphery (Bi), in patterns in certain peripheral parts (Bii), in patches more in the central part (Biii), or as FCLs with a higher degree of connectivity (Biv). The metastatic SW620 cells generally have many FCLs that are organized as patterned FCLs (Ci), or as highly connected rosette-like structures that cover a large portion of the ventral membrane (Cii). Scale bars 5 µm.

KM12C

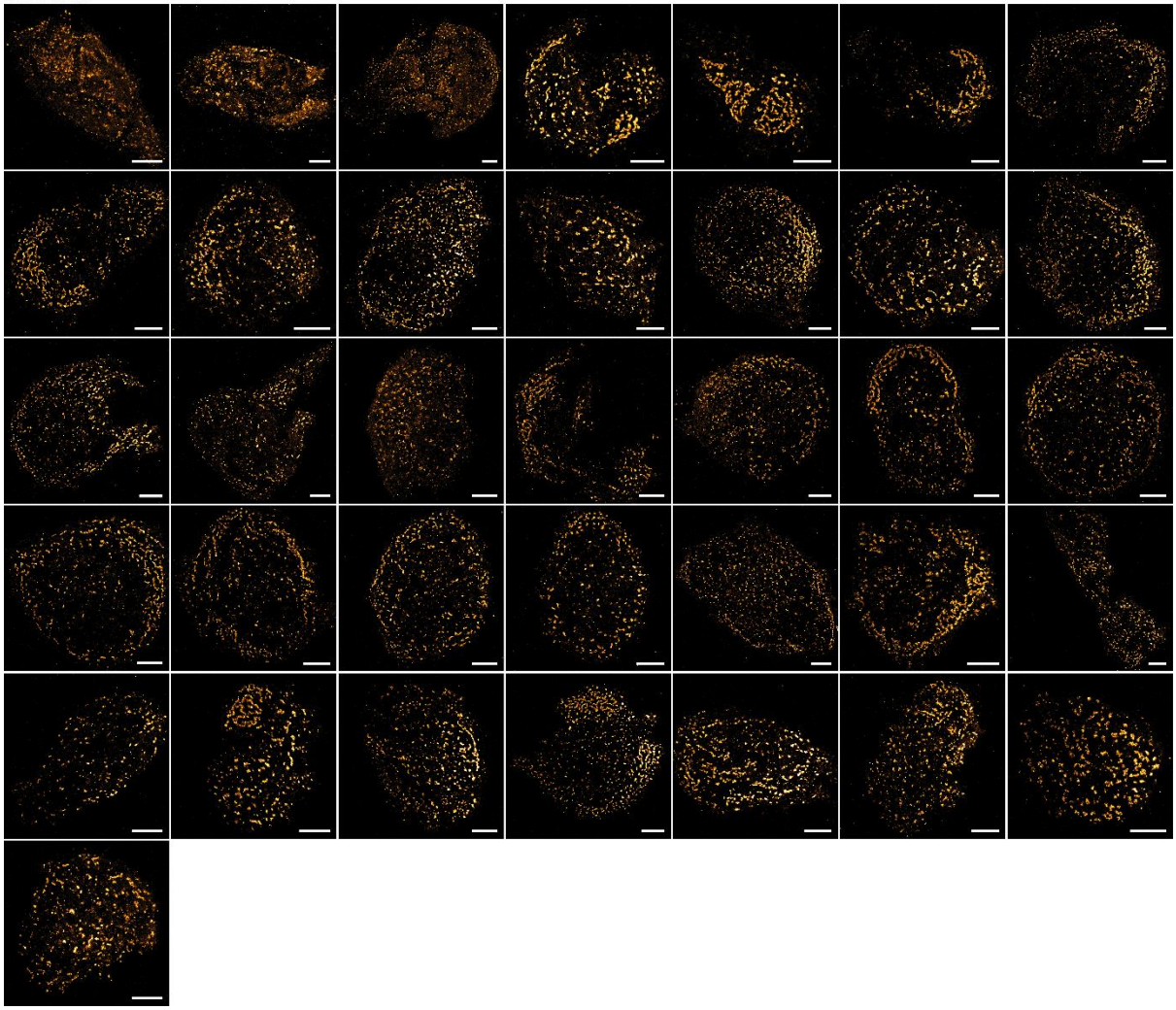

Figure S4: Complete PALM-TIRF dataset of clathrin (mEos3.2-CLTA) imaged at the ventral membrane of KM12C cells, related to Figure 4. Data from at least 7 biological replicates. Images are enlargements of the measured field of view to only contain the cell that was isolated for the analysis where possible. Scale bars 5 µm.

KM12SM

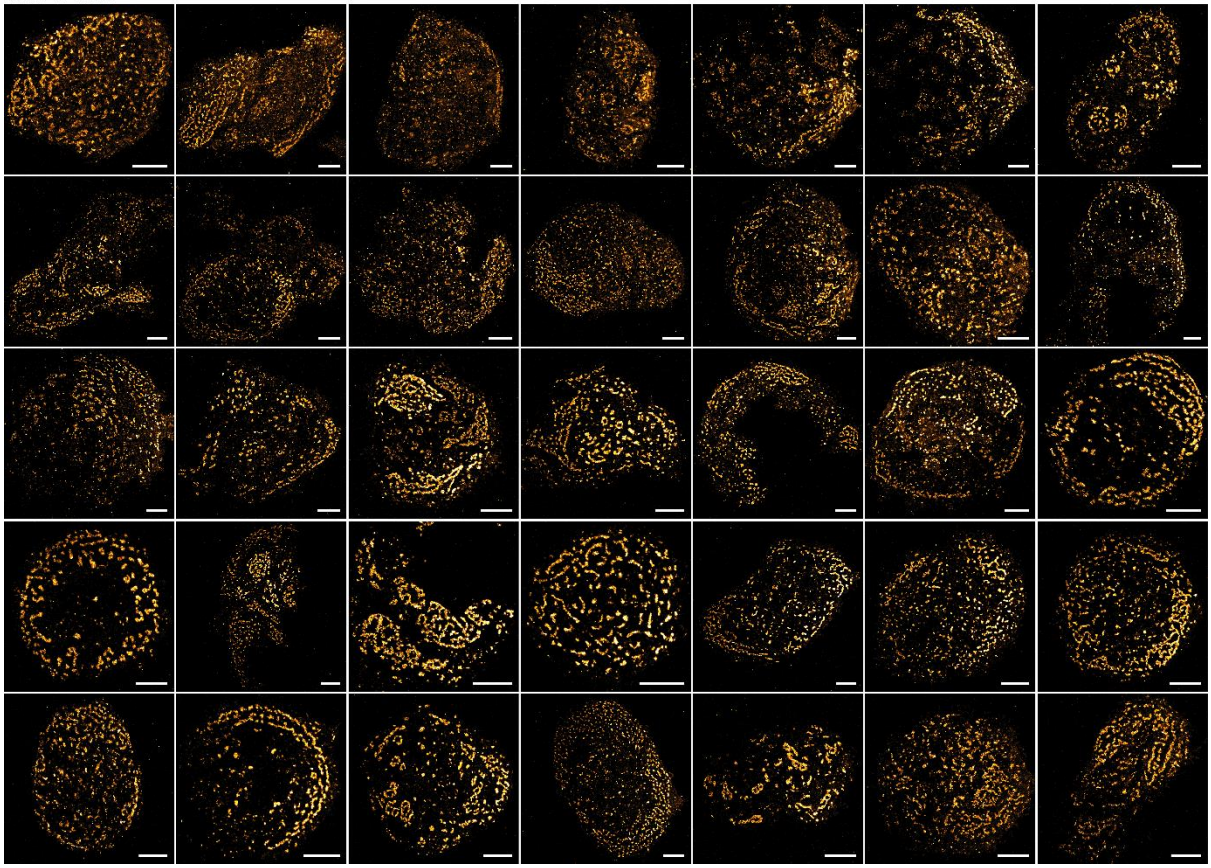

Figure S5: Complete PALM-TIRF dataset of clathrin (mEos3.2-CLTA) imaged at the ventral membrane of KM12SM cells, related to Figure 4. Data from at least 7 biological replicates. Images are enlargements of the measured field of view to only contain the cell that was isolated for the analysis where possible. Scale bars 5 µm.

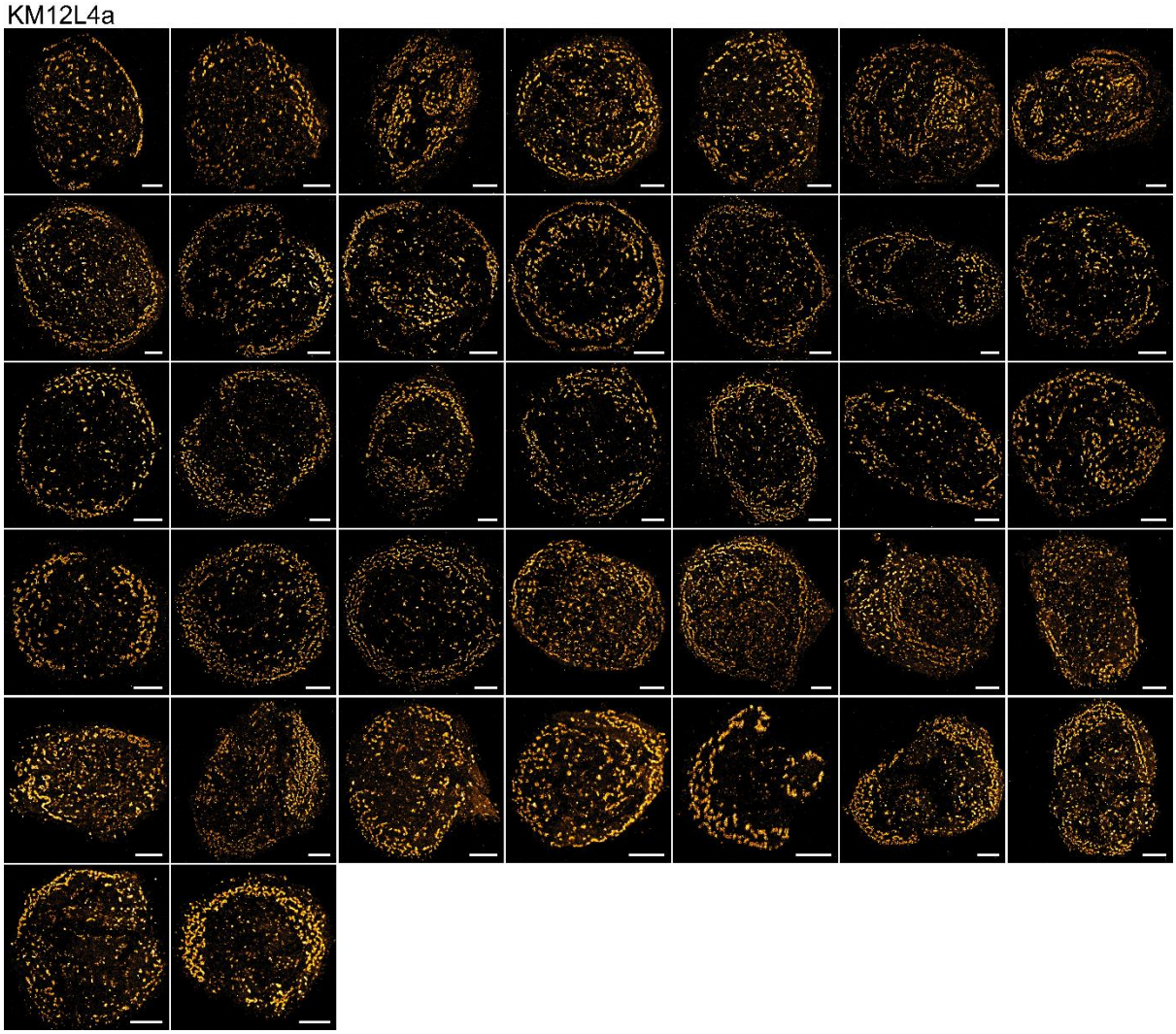

Figure S6: Complete PALM-TIRF dataset of clathrin (mEos3.2-CLTA) imaged at the ventral membrane of KM12L4a cells, related to Figure 4. Data from at least 7 biological replicates. Images are enlargements of the measured field of view to only contain the cell that was isolated for the analysis where possible. Scale bars 5 µm.

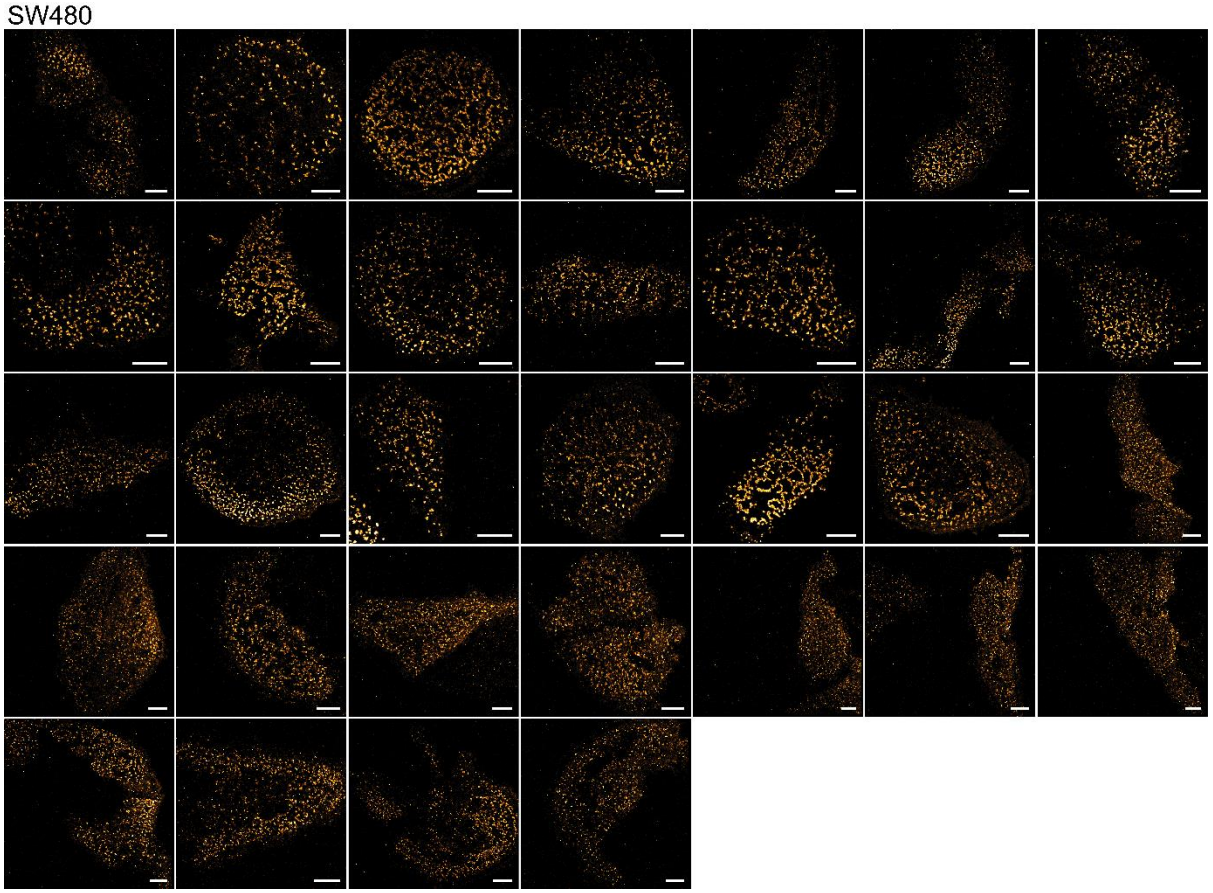

Figure S7: Complete PALM-TIRF dataset of clathrin (mEos3.2-CLTA) imaged at the ventral membrane of SW480 cells, related to Figure 4. Data from at least 7 biological replicates. Images are enlargements of the measured field of view to only contain the cell that was isolated for the analysis where possible. Scale bars 5 µm.

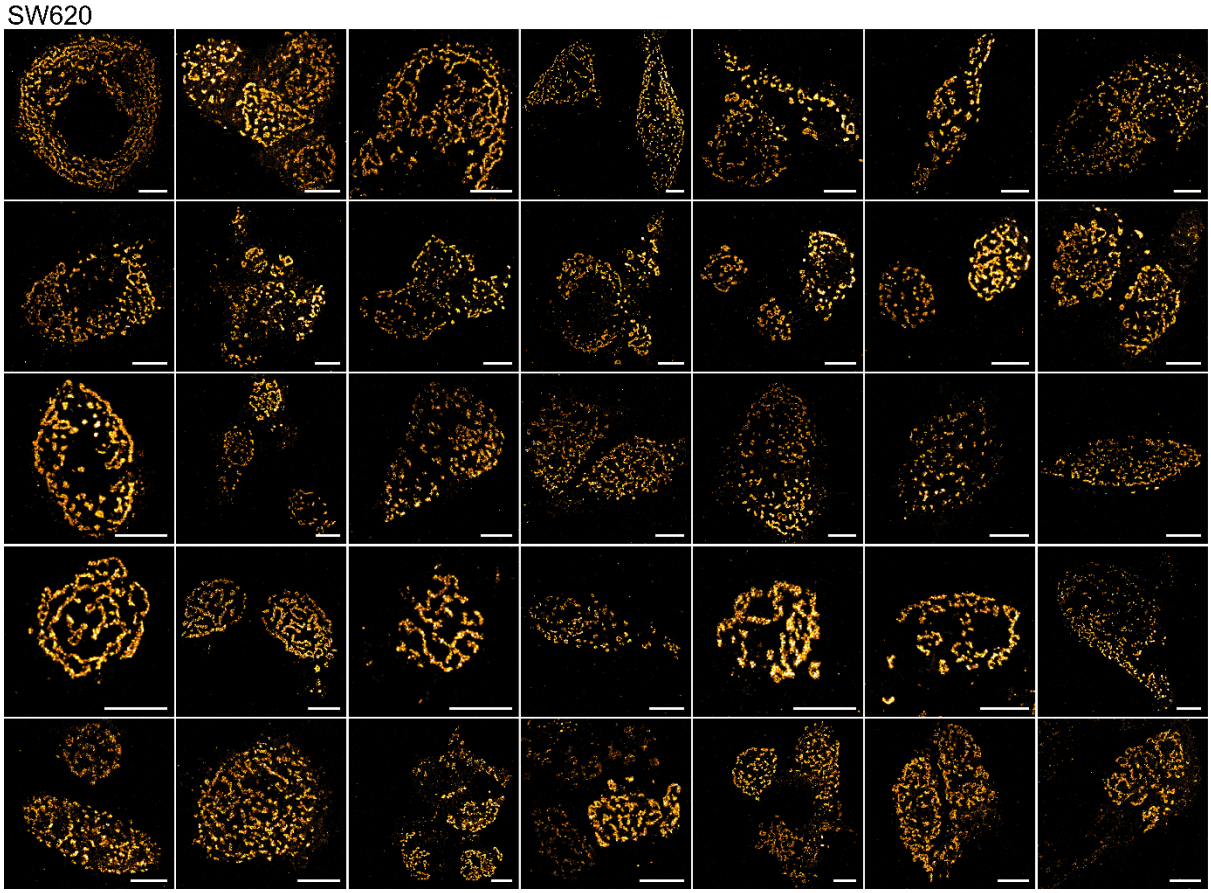

Figure S8: Complete PALM-TIRF dataset of clathrin (mEos3.2-CLTA) imaged at the ventral membrane of SW620 cells, related to Figure 4. Data from at least 7 biological replicates. Images are enlargements of the measured field of view to only contain the cell that was isolated for the analysis where possible. Scale bars 5 µm.

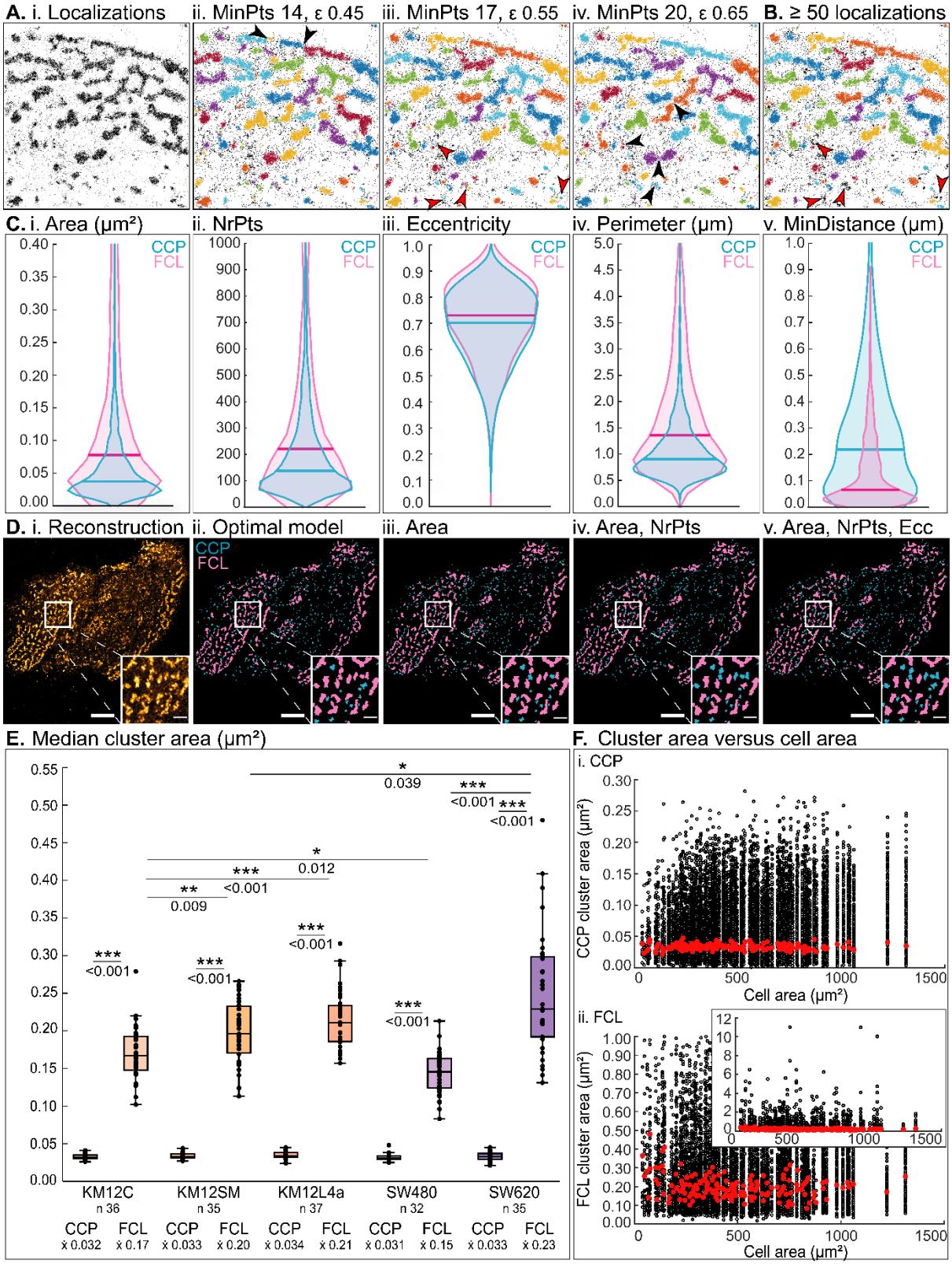

Figure S9: Optimization and testing of the designed cluster classification model, related to Figure 3.

A: Optimization of DBSCAN cluster parameters where minimum number of neighbors (MinPts) and search radius (ε) are optimized (Aii-iv) based on visual observation of a cellular region (Ai). Note that all combinations of MinPts = 8 – 23 and ε = 0.35 – 0.65 were attempted, but that only three parameter combinations are illustrated here. Black arrows indicate examples of suboptimal clustering, where too low DBSCAN parameter values resulted in a cluster being subdivided into smaller segments, and too

high DBSCAN parameter values resulted in individual clusters being merged together. MinPts = 17 and ε = 0.55 (Aiii) were therefore identified as optimal DBSCAN cluster parameters.

B: Justification of the ≥ 50 localization criterium. Clusters that were identified by DBSCAN (Aiii) but have < 50 localizations are not retained for further analysis (examples indicated by red arrows in B and Aiii for comparison). These clusters are extremely small, and their omission does not change our global view of true CCSs.

C: Distribution of cluster characteristics for classical CCSs (blue, indicated as CCP) and alternative FCLs (pink). Cluster characteristics were cluster area (i), the number of localizations within the cluster (ii, NrPts, associated with cluster brightness), the cluster eccentricity (associated with cluster roundness), the cluster perimeter and the distance to the nearest neighboring cluster (MinDistance). These characteristics have a different distribution for classical CCSs and alternative FCLs, and were hence employed in the cluster classification model. Note that FCL distributions and medians are shifted towards higher values compared to classical CCS, except for MinDistance. These relative shifts were accounted for when constructing the classification model (i.e. MinDistance was placed in the denominator of the classification model). Plotted values are derived from 1247 classical CCSs and 1042 alternative FCLs that we manually selected from 3-5 different cellular regions containing predominantly classical CCSs and alternative FCLs, respectively. Violin plots were made using the open-source MATLAB Violin plot function [S1].

D: Illustration of the performance of cluster perimeter and MinDistance (ii) compared to when only considering cluster area (iii); cluster area and NrPts (iv); or cluster area, NrPts and eccentricity (v). Global thresholds for each iteration were determined as performed for the optimized classification model, namely so that maximally 10% of the classical CCSs were misclassified. Scale bars 5 µm, except scale bars of enlargements 1 µm.

E: Median cluster area of classified CCSs per cell. Data are plotted per classified category (CCP for classical CCSs, or FCL) and per cell line. The number of datapoints (n, reflecting the number of cells) and medians ($\tilde{x}$) are provided. Significant differences are calculated for CCP and FCL categories of the same cell line, for relevant CCP categories of different cell lines and for relevant FCL categories of different cell lines. These relevant categories of different cell lines are defined as: KM12C-KM12SM, KM12C-KM12L4a, KM12SM-KM12L4a, SW480-SW620, KM12C-SW480, KM12SM-SW620, KM12L4a-SW620. Statistical significances are shown (* significant difference for $p \leq 0.05$; ** significant difference for $p \leq 0.01$; *** significant difference for $p \leq 0.001$), while non-significant differences ($p > 0.05$) are not displayed.

F: Area of individual CCSs plotted in function of cell area. Separate plots are made for the identified classical CCSs (i) and alternative FCLs (ii), where medians are shown as red dots. Graphs contain PALM-TIRF data from KM12 and SW models, where data is plotted with increasing cell area. While extremely small cells seem to present smaller classical CCSs, there is no significant relationship between classical CCS area and cell area, or between FCL area and cell area. This implies that cluster area does not depend on cell area. Inset for alternative FCLs (ii) shows the true dimensions of the data.

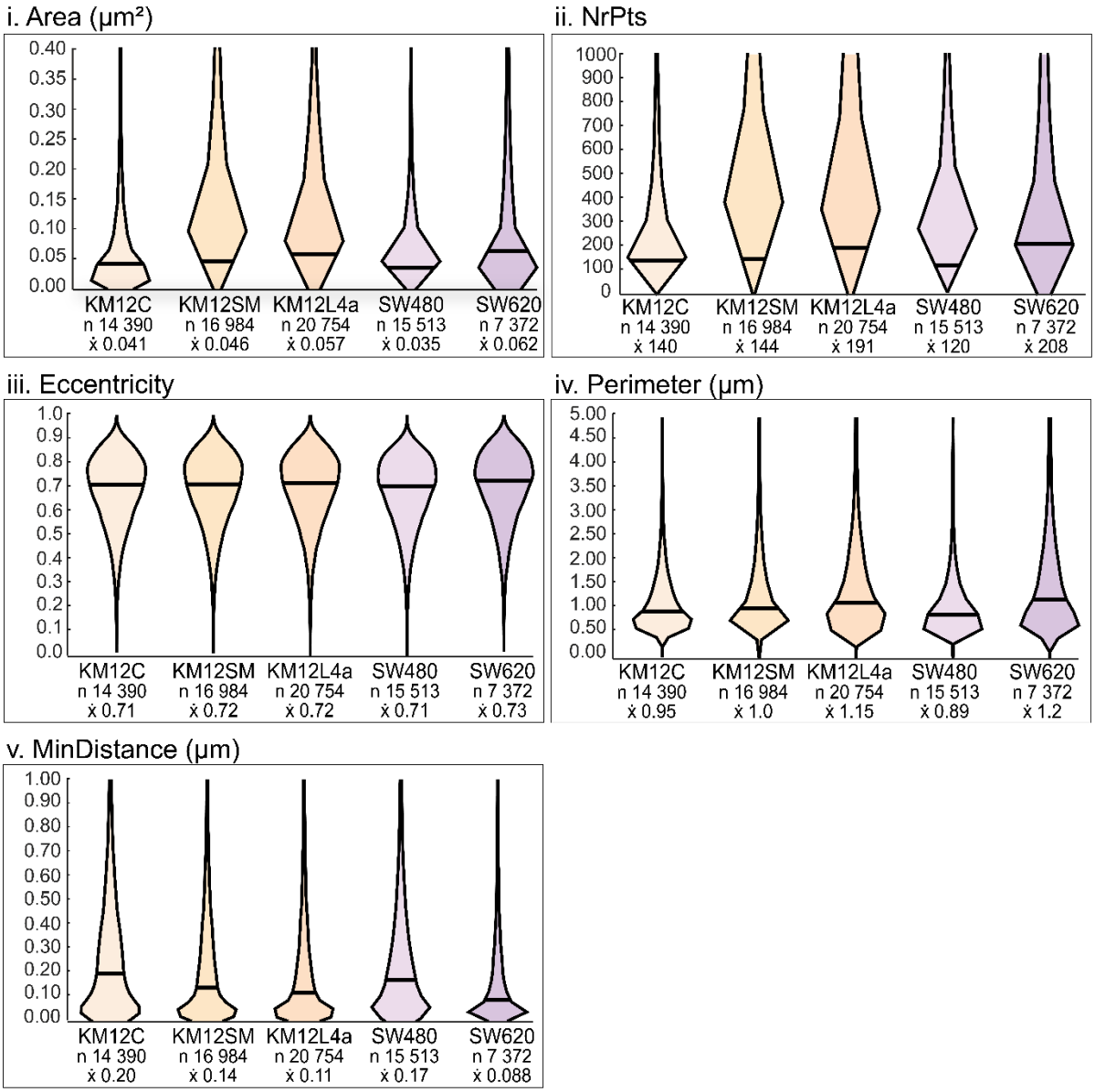

Figure S10: Distribution of cluster characteristics for all identified clusters, arranged per cell line, related to Figure 3. Cluster characteristics were cluster area (i), the number of localizations within the cluster (ii, NrPts, associated with cluster brightness), the cluster eccentricity (associated with cluster roundness), the cluster perimeter and the distance to the nearest neighboring cluster (MinDistance). The number of datapoints (n, reflecting the number of clusters with ≥ 50 localizations) and medians ($\tilde{x}$) are provided. Violin plots were made using the open-source MATLAB Violin plot function [S1].

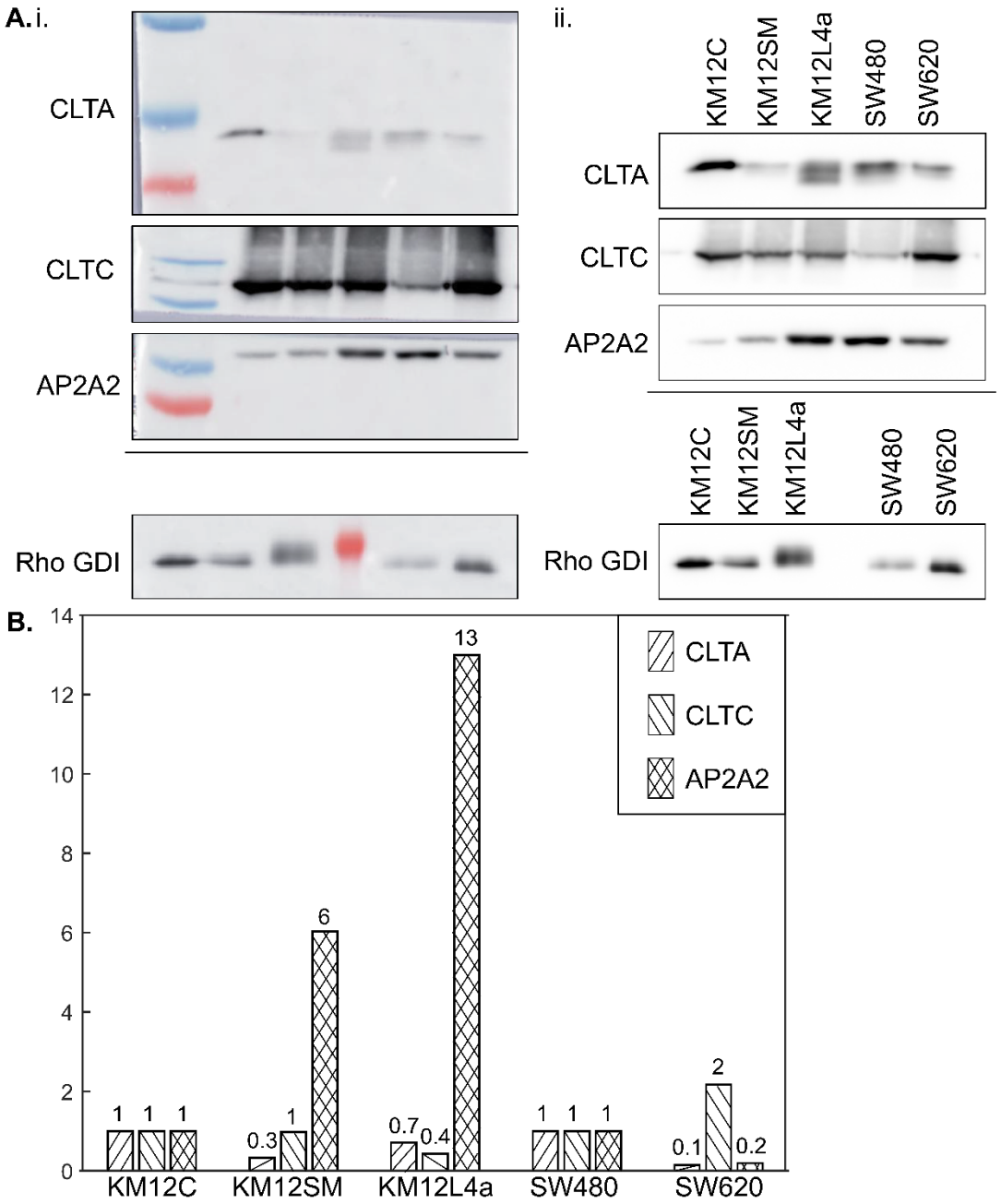

Figure S11: Expression levels of several CME actors, related to Figure 4. Western blot visualization (A) of the different target proteins and Rho GDI which served as loading control. Raw blot data with molecular weight markers visualized (i) and blots with exposure conditions optimized for each target (ii) are shown. Rho GDI results were obtained from a second gel with the same amount of protein extracts loaded. Quantified normalized expression levels obtained from optimized exposure conditions shown in panel Aii (B) were referenced to the poorly metastatic cell line of the corresponding cell model (KM12C for the KM12 model and SW480 for the SW model).

Table S1: Employed reagents for fluorescent labeling of targets in the KM12 and SW cell models, related to STAR Methods and Figure 1-2, Figure 4, Figure S1-S11, and Figure S11.

Western blot	**target**	**primary antibody**	**secondary antibody**
	clathrin light chain A (CLTA) in KM12 or SW cells	rabbit anti-CLTA (Proteintech, 10852-1-AP) 1/1000 dilution	Goat anti-rabbit (GAR)-HRP conjugate (Sigma, A6154) 1/2000 dilution
	clathrin heavy chain 1 (CLTC) in KM12 or SW cells	mouse anti-CLTC (Proteintech, 66487-1-Ig) 1/1000 dilution	Goat anti-mouse (GAM)-HRP conjugate (Sigma, A4416) 1/2000 dilution
	adaptor protein 2, α2-subunit (AP2A2) in KM12 or SW cells	mouse anti-AP2A2 (Santa cruz, sc-55497) 1/1000 dilution	Goat anti-mouse (GAM)-HRP conjugate (Sigma, A4416) 1/2000 dilution
	Rho GDI (protein normalization control) in KM12 or SW cells	mouse anti-Rho GDI (Santa cruz, sc-373724) 1/1000 dilution	Goat anti-mouse (GAM)-HRP conjugate (Sigma, A4416) 1/2000 dilution
Transient transfection	**target**	**plasmid construct**	**transfection conditions**
	clathrin light chain A (CLTA) in KM12 or SW cells	EYFP-CLTA (Addgene, 220921)	0.9 µL TransIT-X2® (Mirus, 6000) 0.3 µg plasmid DNA ~ 0.80 *10^6 cells measurement after ~ 18 hours
	clathrin light chain A (CLTA) in KM12 cells	mEos3.2-CLTA (derived from EYFP-CLTA)	3 µL FuGENE® 6 (Promega, E2691) 0.5 µg plasmid DNA ~ 0.55 * 10^6 cells measurement after ~ 48 hours
	clathrin light chain A (CLTA) in SW cells	mEos3.2-CLTA (derived from EYFP-CLTA)	4.5 µL FuGENE® 6 (Promega, E2691) 0.75 µg plasmid DNA ~ 0.30 * 10^6 cells measurement after ~ 48 hours
Immuno-fluorescence	**target**	**primary antibody**	**secondary antibody**
	clathrin heavy chain 1 (CLTC) in KM12 or SW cells	mouse anti-CLTC (NovusBio, NB300-613) 1/500 dilution	Goat anti-mouse (GAM)-Atto647N (Sigma, 50185) 1/1000 dilution

Table S2: Influence of DBSCAN parameters on clathrin topology quantification: Nr(FCL / classical CCS), values presented in table, for 6 different test cells, related to Figure 3 and Figure S9.

DBSCAN parameters **Cell**	MinPts 14, ε 0.45	MinPts 17, ε 0.55	MinPts 20, ε 0.65
Poorly metastatic KM12C (Fig. 4Ai)	0.147	0.162	0.191
Metastatic KM12SM (Fig. 4Aii)	0.439	0.454	0.472
Metastatic KM12SM (Fig. S3A)	0.603	0.913	0.912
Metastatic KM12L4a (Fig. 4Aiii)	0.287	0.387	0.544
Poorly metastatic SW480 (Fig. 4Aiv)	0.063	0.079	0.106
Metastatic SW620 (Fig. 4Av)	0.591	0.738	1.000

Supplementary Info References

S1. Holger Hoffmann (2022). Violin Plot (https://www.mathworks.com/matlabcentral/fileexchange/45134-violin-plot), MATLAB Central File Exchange. Retrieved October 21, 2022.